Research on Thermal Neutron Shielding Performance of TiB_2-Al Composite Materials

Chao Wang[1]*, Zhefu Li[2], Mengge Dong[3], Lu Zhang[4], Jianxing Liu[3], Xiaozhou Cao[3], and Xiangxin Xue[3]*

[1]Department of Mechanical Engineering, The University of Texas at Dallas, Richardson, TX, 75080, USA
[2]Shanghai Synchrotron Radiation Facility (SSRF), Shanghai Advanced Research Institute, Chinese academy of Sciences, Shanghai, 201204, China
[3]School of Metallurgy, Northeastern University, Shenyang, Liaoning, 110819, China
[4]School of Energy and Environment, Anhui University of Technology, Ma'anshan, 243002, China

Chao Wang, Zhefu Li, and Mengge Dong made an equal contribution.

*Corresponding author. E-mail: wang.chao@utdallas.edu, xuexx@mail.neu.edu.cn

Abstract

Although the various excellent properties and preparation methods of TiB_2-based composites have been extensively studied, their neutron shielding properties have not received as much attention. In this article, the neutron shielding performance of the previously prepared TiB_2-Al composite will be studied. The photo neutron source device was used to carry out neutron irradiation tests on test samples with a thickness of 10 mm. The average thermal neutron shielding rate of TiB_2-based boron-containing composites is 17.55%, and the shielding rate increases with the increase of BN content. The macroscopic cross-section of thermal neutrons of the composites generally shows a stable trend, and when the BN content is 10%, the thermal neutrons macroscopic cross section reaches the maximum value of 7.58cm^{-1}. With the increase of the BN content, the thermal neutron fluence rate shows a gradually decreasing trend.

Keywords: TiB_2, Composites, BN content, Neutron shielding, Shielding rate

Introduction

As one of the modern high-tech materials, boride ceramics are used as hard tool materials, abrasives, alloy additives, and for wear-resistant and corrosion-resistant parts, due to their high melting point, great hardness, high oxidation resistance and high wear resistance (1-5). This kind of material has excellent electrical properties and has been highly valued as an inert electrode material and high temperature electrical material (6-9). The lack of toughness of ceramics is still an urgent problem that needs to be solved (10, 11). One approach is the addition of metal that can improve its toughness and greatly increase its application range (12-14). Among other things, the composite material of boride, combined with plastic or aluminum, produces an effective neutron shielding material (15-19).

Among them, titanium diboride (TiB_2) not only has the properties of high melting point (20, 21), high hardness (22-24), and good high-temperature mechanical properties (25, 26), but it also

has good oxidation resistance (27, 28), strong resistance to chemical corrosion and molten metal corrosion (29, 30), and can resist the corrosion of non-alkali molten salts (31-34). The boron content of TiB_2 is 32.4% . However, to date there has been little research focusing on the use of TiB_2 as an anti-neutron radiation material.

A neutron is a kind of uncharged particle with strong penetrating ability (35, 36). It is one of the rays to which special attention should be paid in matters related to protection. It cannot ionize matter but can ionize matter through secondary particles produced through a process of interaction. Different types of nuclear reactions occur, and the secondary particles produced are also diverse, including gamma photons, alpha particles and so on. The interaction between neutrons and matter is closely related to their energy. Generally, neutron energy is divided into thermal neutrons (below 0.5 eV), medium energy neutrons (0.5 eV～1 keV), fast neutrons (1 keV～10 MeV or 15 MeV), and express neutrons (10 MeV or more than 15 MeV). When a neutron interacts with matter, this interaction mainly occurs with nuclear force in the nucleus and not with the electrons in the outer shell. Neutrons have strong penetrating power when passing through materials, and the danger to the human body is more serious than the same dose of X-rays and γ-rays.

This report was the first direct study of the neutron shielding performance of TiB_2-Al composites with BN added.

Materials and Methods

The TiB_2-Al composite material with BN added is prepared by vacuum infiltration. The amount of BN added is 10% (S1), 20% (S2), 30% (S3), and 40% (S4), more details has been used in previous research (37), and neutron irradiation tests were conducted on test samples with a thickness of 10 mm.

The photo neutron source device driven by the 15 MeV electron accelerator in the Jiading Park of the Shanghai Institute of Applied Physics, Chinese Academy of Sciences (as shown in Figure 1) was used to conduct the thermal neutron irradiation tests on the test samples, and the thermal neutrons of the test samples were carried out with this data shielding performance research. The electron energy of the electron linear accelerator in the device, as stated, is 15 MeV, the pulse width is 3ns-3μs, the pulse frequency is adjustable from 1-266 Hz, and the average pulse current is 0.5mA, and the maximum power is 7.5 kW. The electron beam bombards the tungsten target (W-Tungsten, cylindrical Form) and Gamma rays are generated by bremsstrahlung. Then neutrons are generated through (γ, n) reactions. The peak energy of primary neutrons and gamma rays is about 1MeV. After proper slowing down, the thermal neutrons are continuous. The total yield of neutrons is about 1.2×1011 $n\cdot s^{-1}$, and the neutron flux (neutron flux rate) out of 5 m of the flight path of the Time of Flight (TOF) can reach 105 $n\cdot s^{-1}\cdot cm^{-2}$.

The neutron generation target is a cylindrical, natural tungsten target with a diameter of 60 mm, a thickness of 48 mm, and a purity of 98%. The bottom end is attached to the copper radiator by a special method, as follows. The shell of the target chamber, with a stainless-steel vacuum pipe with an inner diameter of 72.8 mm and a thickness of 5mm, is directly connected to the end of the electron accelerator pipe. The neutron generation target and copper cooling seat are designed and installed with 13 thermocouple thermometers to measure the neutron generation target, and the temperature change of the tube base, while monitoring the displacement of the electron beam on the target. The neutron outlet is equipped with a neutron detector (^{6}LiI crystal), a gamma detector (NaI (TI)), a liquid scintillation detector (EJ301), a 3He proportional counter and a neutron dose

detector. At the end of the TOF path, a ^{6}LiI neutron detector with good shielding is put in place and is used as the TOF neutron time signal termination detector.

Also, MCNP software was used to calculate the thermal neutron energy radiation performance of materials.

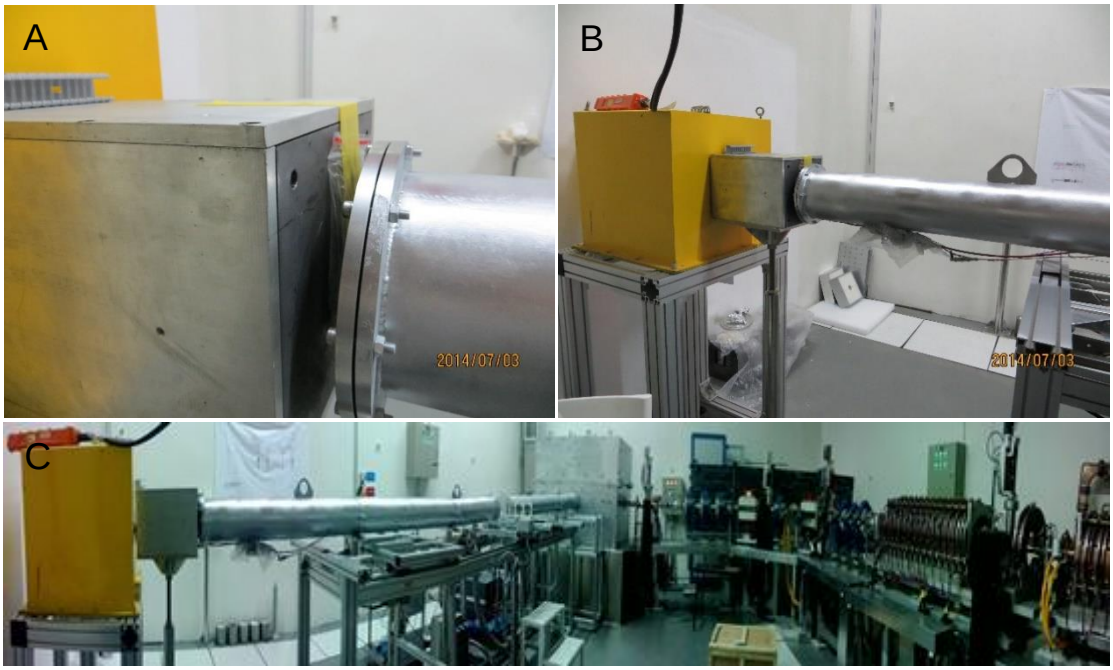

Figure 1: Neutron producing target and photo-neutron facility driven by electron LINAC. **(A)** Neutron producing target. **(B)** Neutron producing target. **(C)** Photo-neutron facility.

Results and Discussion

The attenuation equation of neutrons after passing through the shielding material under collimated narrow beam conditions is:

$$I = I_0 e^{-\Sigma_t d} \tag{1}$$

Among them, I_0 is the intensity of neutrons without shielding material, and I is the intensity of neutrons passing through the shielding material.

The calculation equation of neutron transmittance R_b is:

$$R_b = I / I_0 \tag{2}$$

The calculation equation of the neutron shielding rate R_m is:

$$R_m = (I_0 - I) / I_0 \tag{3}$$

The neutron macroscopic cross section of the composite material satisfies the following relationship:

$$\Sigma(E) = N_A \rho \sum_i \frac{W_i}{WM_i} \sigma_i(E) \quad (4)$$

in which N_A is the Avogadro constant, ρ is the density of the composite material, W_i is the mass of the *i-th* component in the mixture, W is the mass of the mixture, M_i is the molar mass of the *i-th* element, and σ_i is the *i-th* component. The neutron microscopic cross-section of each element is the neutron macroscopic cross-section of the composite material (cm^{-1}).

The effect of the BN content in TiB_2-based composites on thermal neutron transmission and shielding efficiency is shown in Figure 2. Note, with the increase of BN content, the thermal neutron transmittance gradually decreases, and in contrast, the shielding rate of thermal neutrons gradually increases. Calculations indicate the average thermal neutron shielding rate of TiB_2-based composites is 17.55 %. When the BN content is 40%, the shielding effect is at its best, 22.3%.

Figure 2 also demonstrates that when the BN content is between 20% and 30%, the transmittance and shielding rate undergo obvious changes, the transmittance decreases significantly, and the shielding rate increases significantly. When the BN content increases from 30% to 40%, the shielding rate changes very little, with basically no significant increase. This shows that when the BN content of TiB_2 composite material increases to 30%, the shielding rate basically no longer increases, and the shielding effect tends to remain stable.

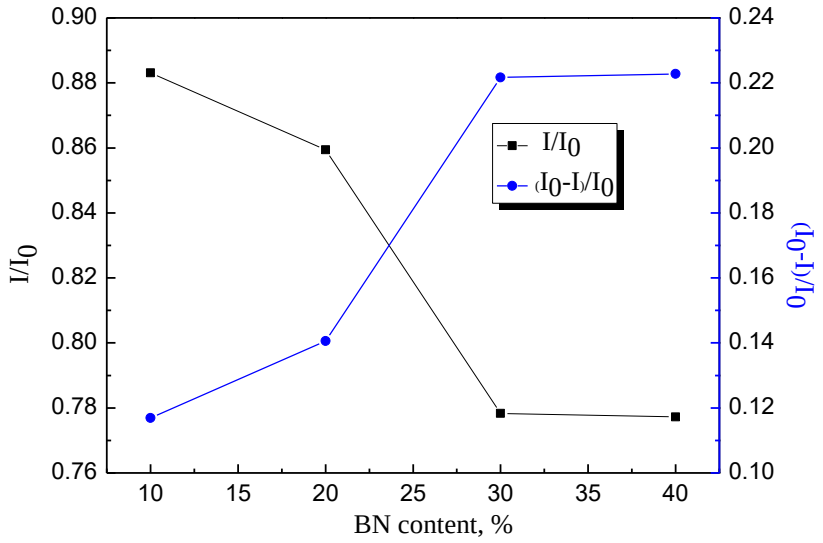

Figure 2 Effect of BN content on the beam ratio I/I_0 and the shield ratio$(I_0-I)/I_0$ of TiB_2 matrix composites.

Figure 3 shows the neutron macroscopic cross-sectional curves of TiB_2-based composites with different BN content drawn according to the calculated results of equation (4). When the BN content increases from 10% to 40%, the neutron macroscopic cross-section of the composite material decreases slightly, but the change range is small, and the overall trend is stable. When the BN content is 10%, the medium of the sub-macroscopic cross-section reaches the maximum value of 7.58 cm^{-1}. It can be seen from equation (4) that the element, element content, and density of the sample have a greater impact on the neutron macroscopic cross-section.

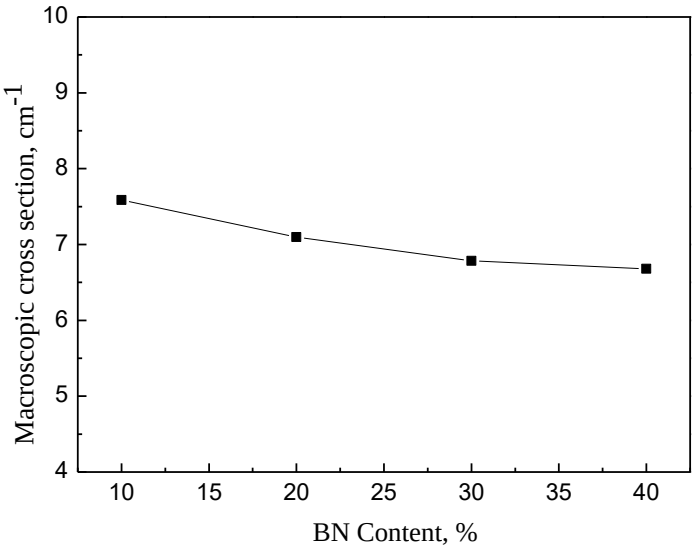

Figure 3 Neutron macroscopic cross sections of TiB_2 matrix composites with different BN content.

Table 1 shows the element content and density of TiB_2-based boron-containing composite materials. The thermal neutron absorption cross-section of boron (B) is 759 barn, while the other elements are much lower than boron (Ti: 6.1 barn, N: 1.85 barn, Al: 0.23 barn). This shows that the main effect of the macroscopic cross-section is boron. The boron content in the four samples does not change much, and the density change is also very small. This shows that the thermal neutron macroscopic cross-section of the TiB_2-based boron-containing composite material changes, and this change is affected by the combination of the element content and density.

Table 1 Element content and density of TiB_2 matrix composites materials

Samples	Ti (%)	B (%)	N (%)	Al (%)	Density ($g \cdot cm^{-3}$)
S1	37.66	22.34	6.57	33.44	3.69
S2	31.24	21.57	9.31	37.88	3.57
S3	25.17	20.52	11.51	42.80	3.59
S4	21.44	21.06	14.35	43.15	3.44

Figure 4 is a macroscopic cross-sectional view of thermal neutrons of TiB_2-based composite materials irradiated with different thermal neutron energies drawn according to the calculated results of MCNP software. The macroscopic cross-sectional change trends of thermal neutrons of S1~S4 are almost the same, with little difference. With the increase of radiation intensity, the macroscopic cross-sections of thermal neutrons of S1~S4 gradually decrease, with obvious fluctuations in the range of 0.1~0.5MeV.

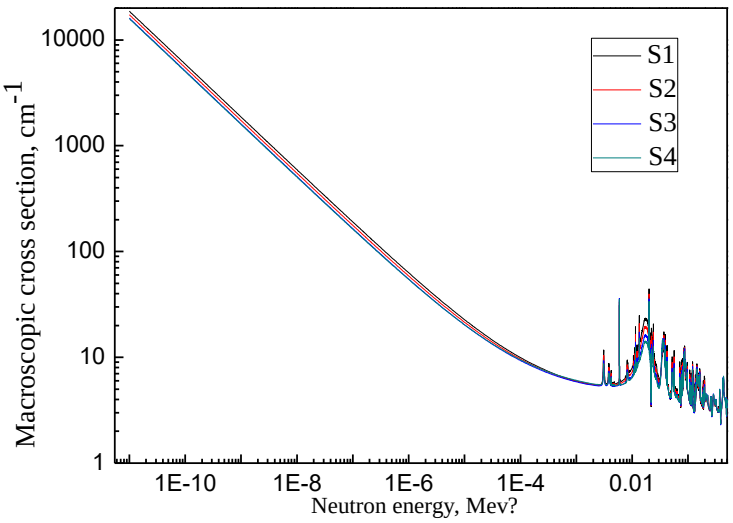

Figure 4 Neutron macroscopic cross sections of TiB_2 matrix composites.

The neutron fluence rate refers to the quotient obtained by dividing the number of neutrons received in a unit of time into a small sphere, centered at that point in any direction at a certain point in space, by the maximum cross-sectional area of the sphere. In other words, it is the number of neutrons entering or passing through a unit cross-sectional area of a sphere with a unit surface area in a unit of time. The neutron fluence rate is also called neutron flux. The measurement of neutron fluence rate is an inevitable link in the research and application of neutron physics. Figure 5 shows the relationship between the content of each element in the composite material and the neutron fluence rate.

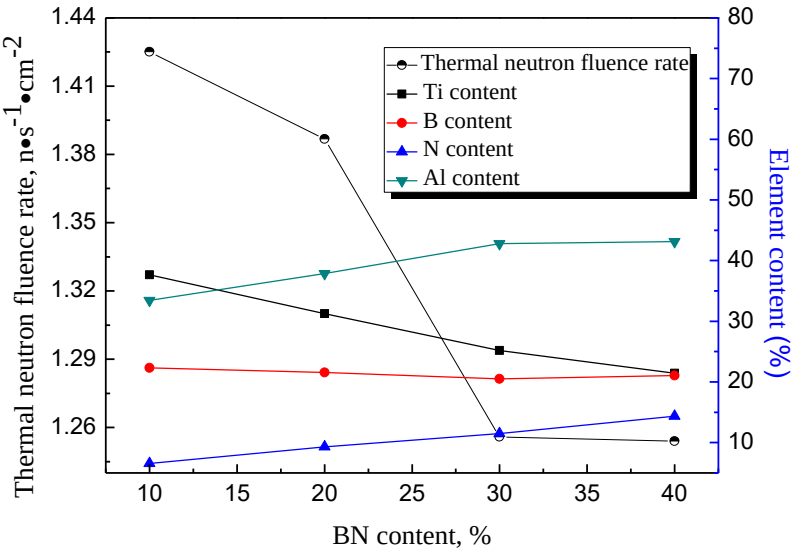

Figure 5 The relationship between thermal neutron flux rate and content variations of the main elements in the composites.

It can be observed from Figure 5 that with the increase of BN content, the thermal neutron fluence rate decreases from 1.43 to 1.25 $n \cdot s^{-1} \cdot cm^{-2}$. This decrease shows that under the same neutron source irradiation, with the increase of BN content, the thermal neutron fluence rate gradually decreases, meaning, the neutron transmittance per unit area gradually decreases. Table 2 lists the BN content in TiB_2-based composites and its corresponding thermal neutron fluence rate.

Table 2 BN content and thermal neutron flux rate ($n \cdot s^{-1} \cdot cm^{-2}$) of composites

Content of BN	10%	20%	30%	40%
Thermal neutron fluence rate	1.43	1.39	1.26	1.25

Summary

The average thermal neutron shielding rate of the TiB_2-based boron-containing, composite material with a thickness of 10mm is 17.55 percent, and the shielding rate increases with the increase of the BN content. The thermal neutron cross section of the composite material generally remains stable. When the BN content is 10%, the thermal neutron macroscopic cross-section reaches its maximum value of $7.58cm^{-1}$. With the increase of BN content, the thermal neutron fluence rate tends to gradually decrease.

Notes

The authors declare that they have no competing financial interest.

Acknowledgements

This work was supported by the fundamental, scientific-research business resources of the central universities (award # N10060200).

References

1. V. I. Matkovich, *Boron and refractory borides* (Springer, 1977).
2. C. Wang *et al.* (2014) Elementary research on preparation of AlB_{12} powder by self-propagating high-temperature synthesis (SHS). in *Materials Science Forum* (Trans Tech Publ), pp 365-369.
3. X. Cao, C. Wang, X. Xue, H. Yang, Preparation of tungsten boride ceramic by pressureless sintering. *Journal of Inorganic Materials* **29**, 498-502 (2014).
4. C. Wang, M. E. Hossain Bhuiyan, S. Moreno, M. Minary-Jolandan, Direct-Write Printing Copper–Nickel (Cu/Ni) Alloy with Controlled Composition from a Single Electrolyte Using Co-Electrodeposition. *ACS Applied Materials & Interfaces* **12**, 18683-18691 (2020).

5. M. Mahmoudi *et al.*, Three-Dimensional Printing of Ceramics through "Carving" a Gel and "Filling in" the Precursor Polymer. *ACS Applied Materials & Interfaces* **12**, 31984-31991 (2020).
6. W. Tao *et al.* (2009) Finite element analysis of thermo-electric coupled field in 400kA large-scale aluminum reduction cell. in *2009 World Non-Grid-Connected Wind Power and Energy Conference* (IEEE), pp 1-4.
7. J. Hu, M.-F. Yu, Meniscus-confined three-dimensional electrodeposition for direct writing of wire bonds. *Science* **329**, 313-316 (2010).
8. X. Cao *et al.* (2011) High temperature electrochemical synthesis of tungsten boride from molten salt. in *Advanced Materials Research* (Trans Tech Publ), pp 463-466.
9. Q. Li *et al.*, High-temperature dielectric materials for electrical energy storage. *Annual Review of Materials Research* **48**, 219-243 (2018).
10. C. Wang *et al.*, Preparation of AlB_{12} Powder by Self-Propagating High-Temperature Synthesis (SHS). https://doi.org/10.26434/chemrxiv.13591313.v1. (2021).
11. K. Liang, G. Orange, G. Fantozzi, Evaluation by indentation of fracture toughness of ceramic materials. *Journal of Materials Science* **25**, 207-214 (1990).
12. J. Huang, S. Daryadel, M. Minary-Jolandan, Low-Cost Manufacturing of Metal–Ceramic Composites through Electrodeposition of Metal into Ceramic Scaffold. *ACS applied materials & interfaces* **11**, 4364-4372 (2019).
13. D. Qi *et al.*, Preparation and Erosion Performance for Co-continuous Phase Composites of Si_3N_4/1Cr18Ni9Ti. *Chinese Journal of Materials Research* **33**, 34-42 (2019).
14. S. Suresh, N. Shenbag, V. Moorthi, Aluminium-titanium diboride (Al-TiB2) metal matrix composites: challenges and opportunities. *Procedia Engineering* **38**, 89-97 (2012).
15. M. Dong *et al.*, A novel comprehensive utilization of vanadium slag: as gamma ray shielding material. *Journal of hazardous materials* **318**, 751-757 (2016).
16. X. Cao, C. Wang, X. Xue, G. Cheng, Effect of ti addition on the residual aluminium content and mechanical properties of the B_4C-al composites produced by vacuum infiltration. *Archives of Metallurgy and Materials* **60**, 2493-2398 (2015).
17. Z. Xu *et al.*, The design of a novel neutron shielding B_4C/Al composite containing Gd. *Materials & Design* **111**, 375-381 (2016).
18. N. Tariq *et al.*, Cold spray additive manufacturing: A viable strategy to fabricate thick B_4C/Al composite coatings for neutron shielding applications. *Surface and Coatings Technology* **339**, 224-236 (2018).
19. M. Dong *et al.*, Preparation, shielding properties and mechanism of a novel neutron shielding material made from natural Szaibelyite resource. *Progress in Nuclear Energy* **106**, 140-145 (2018).
20. X.-w. Hu *et al.* (2007) Nd_2O_3 Solubility in NdF_3-LiF-Nd_2O_3 Melts. in *Proceedings of NGCWP 2007*.
21. X. Luo *et al.*, Influence of metallic additives on densification behaviour of hot-pressed TiB_2. *Light Metals*, 1151-1155 (2009).
22. X. Cao *et al.*, Effect of Ni addition on pressureless sintering of tungsten diboride. *International Journal of Refractory Metals and Hard Materials* **41**, 597-602 (2013).
23. X. Cao *et al.*, Electrochemical Behavior and Electrodeposition of Sn Coating from Choline Chloride–Urea Deep Eutectic Solvents. *Coatings* **10**, 1154 (2020).

24. E. W. Neuman, H. J. Brown-Shaklee, G. E. Hilmas, W. G. Fahrenholtz, Titanium diboride–silicon carbide–boron carbide ceramics with super-high hardness and strength. *Journal of the American Ceramic Society* **101**, 497-501 (2018).
25. C. Wang, J. Zhang, X. X. Xue, X. Z. Cao (2013) Fabrication B-Ni-Al Shielding Materials by Vacuum Metal Infiltration. in *Advanced Materials Research* (Trans Tech Publ), pp 410-413.
26. J. Oñoro, High-temperature mechanical properties of aluminium alloys reinforced with titanium diboride (TiB 2) particles. *Rare Metals* **30**, 200 (2011).
27. C. Wang, X. Xue, X. Cao, H. Yang, G. Cheng, The effect of Ti addition on the microstructure and fracture toughness of BN-Al composite materials synthesized by vacuum infiltration. *Archives of Metallurgy and Materials* **58**, 509-512 (2013).
28. E. Clougherty, R. Pober, L. Kaufman (1968) Synthesis of oxidation resistant metal diboride composites. (ManLabs., Inc., Cambridge, Mass.).
29. C. WANG *et al.*, Research Progress on Aluminum-Boron Compounds (Al-B) and Its Composite Materials. *Bulletin of the Chinese Ceramic Society*, 26 (2013).
30. C. Monticelli, A. Frignani, A. Bellosi, G. Brunoro, G. Trabanelli, The corrosion behaviour of titanium diboride in neutral chloride solution. *Corrosion science* **43**, 979-992 (2001).
31. C. Wang *et al.*, A New Method of Fabricating AlN-TiB_2 Composite Ceramics. *Materials and manufacturing processes* **28**, 953-956 (2013).
32. S. Lakshmi, L. Lu, M. Gupta, In situ preparation of TiB_2 reinforced Al based composites. *J Mater Process Tech* **73**, 160-166 (1998).
33. C. Wang *et al.*, Theoretical Calculation of Self-Propagating High-Temperature Synthesis (SHS) Preparation of AlB_{12}. https://doi.org/10.26434/chemrxiv.13591427.v1. (2021).
34. L. M. Sworts, Dynamic Fatigues Testing of Titanium Diboride in Molten Aluminum. (2012).
35. F. H. Attix, *Introduction to radiological physics and radiation dosimetry* (John Wiley & Sons, 2008).
36. S. Youwu, L. Wuyuan, X. Junkui, M. Wang, L. Zongqiang, Neutron influence in charged particle therapy. *Modern Practices in Radiation Therapy, In Tech, Rijeka*, 85-112 (2012).
37. C. Wang, X. Xue, X. Cao, H. Yang, Effect of BN Addition on Mechanical Properties and Microstructure of TiB_2-Al Composites. *Journal of Northeastern University (Natural Science)*, 19 (2012).